

Anisotropic electronic and excitonic properties of monolayer SiP_2 from the first-principles GW-BSE calculations

Zichen Wang(王紫辰), Benshu Fan(范本澍), and Peizhe Tang(汤沛哲)
Citatio: Chin. Phys. B, 2025, 34 (**9**): 097801. DOI: 10.1088/1674-1056/ade66a
http://cpb.iphy.ac.cn; http://iopscience.iop.org/cpb

What follows is a list of articles you may be interested in

Temperature-dependent photoluminescence of lead-free cesium tin halide perovskite microplates

Jiayu Tan(谭佳雨), Yixuan Zhou(周译玄), De Lu(卢德), Xukun Feng(冯旭坤), Yuqi Liu(刘玉琪), Mengen Zhang(张蒙恩), Fangzhengyi Lu(卢方正一), Yuanyuan Huang(黄媛媛), and Xinlong Xu(徐新龙)
Chin. Phys. B, 2023, 32 (**11**): 117802. DOI: 10.1088/1674-1056/ad028e

Anomalous photoluminescence enhancement and resonance charge transfer in type-II 2D lateral heterostructures

Chun-Yan Zhao(赵春艳), Sha-Sha Li(李莎莎), and Yong Yan(闫勇)
Chin. Phys. B, 2023, 32 (**8**): 087801. DOI: 10.1088/1674-1056/acc1d1

Enhanced photoluminescence of monolayer MoS_2 on stepped gold structure

Yu-Chun Liu(刘玉春), Xin Tan(谭欣), Tian-Ci Shen(沈天赐), and Fu-Xing Gu(谷付星)
Chin. Phys. B, 2022, 31 (**8**): 087803. DOI: 10.1088/1674-1056/ac657b

Exciton luminescence and many-body effect of monolayer WS_2 at room temperature

Jian-Min Wu(吴建民), Li-Hui Li(黎立辉), Wei-Hao Zheng(郑玮豪), Bi-Yuan Zheng(郑弼元), Zhe-Yuan Xu(徐哲元), Xue-Hong Zhang(张学红), Chen-Guang Zhu(朱晨光), Kun Wu(吴琨), Chi Zhang(张弛), Ying Jiang(蒋英),Xiao-Li Zhu(朱小莉), and Xiu-Juan Zhuang(庄秀娟)
Chin. Phys. B, 2022, 31 (**5**): 057803. DOI: 10.1088/1674-1056/ac380c

Magnetic polaron-related optical properties in Ni(II)-doped CdS nanobelts: Implication for spin nanophotonic devices

Fu-Jian Ge(葛付建), Hui Peng(彭辉), Ye Tian(田野), Xiao-Yue Fan(范晓跃), Shuai Zhang(张帅), Xian-Xin Wu(吴宪欣), Xin-Feng Liu(刘新风), and Bing-Suo Zou(邹炳锁)
Chin. Phys. B, 2022, 31 (**1**): 017802. DOI: 10.1088/1674-1056/ac0782

SPECIAL TOPIC — Exciton physics: Fundamentals, materials and devices

Anisotropic electronic and excitonic properties of monolayer SiP_2 from the first-principles GW-BSE calculations

Zichen Wang(王紫辰)[1], Benshu Fan(范本澍)[2,†], and Peizhe Tang(汤沛哲)[1,2,‡]

[1] *School of Materials Science and Engineering, Beihang University, Beijing* 100191, *China*
[2] *Max Planck Institute for the Structure and Dynamics of Matter, Luruper Chaussee* 149, 22761 *Hamburg, Germany*

(Received 13 May 2025; revised manuscript received 20 June 2025; accepted manuscript online 20 June 2025)

We investigate electronic structures and excitonic properties of monolayer SiP_2 within the framework of first-principles GW plus Bethe–Salpeter equation (GW-BSE) calculations. Within the G_0W_0 approximation, monolayer SiP_2 is identified as a direct-gap semiconductor with an electronic gap of 3.14 eV, and the excitons exhibit a hybrid-dimensional character similar to that of the bulk counterpart. The optical absorption spectra reveal pronounced excitonic effects with strong anisotropy: the first bright exciton has a binding energy of 840 meV under *x*-polarized light, compared with 450 meV under *y*-polarized light. We further analyze the symmetry origins of the polarization-dependent optical selection rules through group theory. This binding energy difference arises from the intrinsic nature of the excitons: flat-band excitons under *x*-polarized light and conventional excitons localized at a single $\boldsymbol{k}$ point under *y*-polarized light. Our work enhances the understanding of excitonic behavior in monolayer SiP_2 and highlights its potential for polarization-sensitive and directionally tunable optoelectronic applications.

Keywords: hybrid dimensionality, exciton, GW-BSE

PACS: 78.66.–w

DOI: 10.1088/1674-1056/ade66a **CSTR:** 32038.14.CPB.ade66a

1. Introduction

Due to the widespread applications of photoelectric devices in various fields, the optical properties of layered materials have garnered significant attention.[1–6] Excitons, which are quasi-particles formed by bound electron–hole pairs, play a critical role in determining the optical property of the semiconductor. Notably, excitonic behavior is highly sensitive to the dimensionality of the host material. In two-dimensional (2D) semiconductors, excitonic properties differ markedly from their bulk counterparts, primarily due to the reduced Coulomb screening in low-dimensional systems.[7,8] This phenomenon leads to a substantial enhancement in excitonic binding energy, thereby amplifying the influence of excitonic effects on the optical properties of 2D semiconductors, such as transition metal dichalcogenides (TMDs),[9–19] divanadium pentaoxide (V_2O_5),[20,21] silicon diphosphorus (SiP_2)[22–26] and so on.[27–33] Consequently, a comprehensive understanding of these excitonic features is crucial for leveraging the unique optical properties of 2D materials in optoelectronic applications.

As a prototypical class of van der Waals layered materials, TMDs have been extensively explored for their potential in optoelectronic applications.[9–19] In particular, monolayer MoS_2 has attracted considerable interest due to its prominent excitonic effects. The GW-BSE calculations reveal a direct electronic band gap of 2.67 eV and the first bright exciton with a binding energy of 0.63 eV, which is primarily contributed by the band edge states at the *K* point of the Brillouin zone (BZ) in monolayer MoS_2.[16,17] Owing to the nearly isotropic in-plane screening, the excitonic wavefunctions in MoS_2 resemble those of the hydrogen atom, following conventional optical selection rules for s-, p-, and d-like excitonic series.[18] Another TMD material, monolayer WSe_2, has been proposed as a potential excitonic insulator, where a Fulde–Ferrell–Larkin–Ovchinnikov (FFLO)-like state emerges due to its unique excitonic band structure, favoring stripe-patterned topological exciton density waves with finite momentum.[19] Beyond TMDs, materials with flat band structures have also attracted attention. In V_2O_5, both conduction band (CB) and valence band (VB) around the Fermi level are nearly flat across the BZ, enabling exciton formation at a wide range of $\boldsymbol{k}$-points rather than just at the band edges. Such exotic property with flat band dispersion leads to highly delocalized excitonic states in the momentum space and increases their binding energy correspondingly. Remarkably, the binding energy of bulk V_2O_5 reaches an extremely large value up to 1.6 eV.[20,21,34]

Some other layered materials with distinct crystal structures also exhibit unique excitonic behaviors. SiP_2, for exam-

†Corresponding author. E-mail: benshu.fan@mpsd.mpg.de
‡Corresponding author. E-mail: peizhet@buaa.edu.cn

© 2025 Chinese Physical Society and IOP Publishing Ltd. All rights, including for text and data mining, AI training, and similar technologies, are reserved.

ple, has two bulk polymorphs that share the same monolayer building blocks but differ in their stacking arrangements.[22–26] As shown in Fig. 1(a), each SiP_2 monolayer contains a substructure composed of the chain-like phosphorus atoms, giving rise to strong in-plane anisotropy. Our previous work has investigated the electronic structures and optical properties of one polymorph with space group *Pnma* (No. 62) based on the GW-BSE calculations.[25] We identified it as a semiconductor with the indirect band gap of 2.14 eV and the first bright exciton with a binding energy of 140 meV, which can be only excited by incident light polarized perpendicular to the phosphorus atom chains. Additionally, analysis of the excitonic wavefunction revealed that this bright exciton is hybrid-dimensional, comprising one-dimensional (1D) electrons along the phosphorus atom chains and 2D holes across the monolayer plane. In a separate study, Matta *et al.*[26] further reported that monolayer SiP_2 possesses a band gap of 2.63 eV and an excitonic binding energy of 610 meV without fully including the low-dimensional screening effect.[35] Their results also revealed a strong anisotropy in the band structures, featuring a flat band along the Γ–X direction and markedly steeper dispersion along Γ–Y, indicating an excitonic behavior distinct from that in MoS_2 and V_2O_5. These findings motivate a more in-depth investigation of the excitonic properties in monolayer SiP_2, with attention to the detailed treatment of long-range Coulomb interactions in 2D systems.

In this work, we present a detailed investigation of the electronic band structures and excitonic properties of monolayer SiP_2 using the GW-BSE method. We demonstrate its large exciton binding energy and highly anisotropic optical responses. Moreover, we analyze the polarization-dependent optical selection rules based on group theory and visualize the excitonic wavefunctions in both reciprocal and real spaces. These findings provide insight into the hybrid-dimensional and polarization-dependent excitonic behaviors in monolayer SiP_2, highlighting its potential for applications in anisotropic optoelectronic devices.

2. Computational details

We employ density functional theory (DFT) calculations implemented in the Quantum ESPRESSO package[36] to determine the optimized structure and electronic band structure of monolayer SiP_2. The Kohn–Sham (KS) orbitals are expanded using a plane-wave basis with a cutoff energy of 80 Ry, and the Brillouin zone (BZ) is sampled using a Γ-centered $6 \times 14 \times 1$ $\boldsymbol{k}$-grid, following the Monkhorst–Pack (MP) method. The self-consistent calculations are carried out with a convergence threshold of 1×10^{-12} Ry, and the structural optimizations achieve a stringent tolerance of 1×10^{-4} Ry/Bohr. We adopt the generalized gradient approximation (GGA) with the Perdew–Burke–Ernzerhof (PBE) functional to describe the exchange–correlation energy, while the interactions between valence and core electrons are modeled using SG15 optimized norm-conserving vanderbilt (ONCV) pseudopotentials.[37,38] Additionally, the IrRep code[39] is utilized to analyze the symmetry of the electronic Bloch states.

We then refine the KS one-electron energies using G_0W_0 (one-shot) self-energy corrections implemented in the YAMBO code,[40,41] based on the DFT-PBE ground-state results. To mitigate the divergence of the 2D Coulomb potential at small $\boldsymbol{k}$, we employ the random integration method (RIM) with Monte Carlo integration across randomly sampled $\boldsymbol{k}$ points.[42] Our calculations achieve convergence using 422 unoccupied states and a slab-plane truncation of the bare Coulomb potential.[35] To account for electron–hole interactions, we employ the Bethe–Salpeter equation (BSE) for the two-particle correlation function, incorporating prior GW corrections. Our GW-BSE calculations adopt the Tamm–Dancoff approximation, which accurately describes excitonic effects in semiconductors.[43] To improve numerical precision, the BSE kernel is initially computed on a coarse $\boldsymbol{k}$-grid ($6 \times 14 \times 1$) and subsequently interpolated onto a finer grid ($12 \times 28 \times 1$). The absorption spectrum is determined by ε_2, which represents the imaginary part of the macroscopic dielectric function.

3. Results and discussion

The anisotropic crystal structure of monolayer SiP_2, illustrated in Fig. 1(a), features two distinct types of phosphorus atoms. The P_A atoms form a 2D network with silicon atoms, while the P_B atoms align into quasi-1D chains along the y direction. This structural anisotropy leads to distinctive electronic properties. As shown in Fig. 1(b), the electronic band structures from the G_0W_0 approximation exhibit a nearly rigid upward shift compared to results with the GGA-PBE functional, indicating that monolayer SiP_2 is a direct gap semiconductor with a band gap of 3.14 eV. Notably, the discrepancy between band gaps from the G_0W_0 and GGA-PBE functional is more pronounced in the monolayer SiP_2 than that in the bulk, primarily due to reduced dielectric screening and the enhanced quantum confinement in 2D systems. Moreover, both the highest VB and the lowest CB are relatively flat along the Γ–X direction, suggesting a certain degree of localization for the electrons and holes involved in exciton formation. To further elucidate the nature of these electronic states, we examine the real-space charge density distributions of the valence band maximum (VBM) and the conduction band minimum (CBM), as shown in Figs. 1(c) and 1(d). The charge density of the VBM is extended over the quasi-2D atomic plane, whereas that of the CBM is primarily localized along the P_B–P_B chains,

indicating a quasi-1D character. This spatial anisotropy suggests that excitons in monolayer SiP_2 exhibit hybrid dimensionality, similar to their bulk counterparts,[24] which arises mainly from the nature of chemical bonding and remains robust against van der Waals interactions. Moreover, the hybrid-dimensional nature of excitonic states may play a role in determining the properties of interlayer excitons in the van der Waals heterostructures, which deserves further exploration.[44]

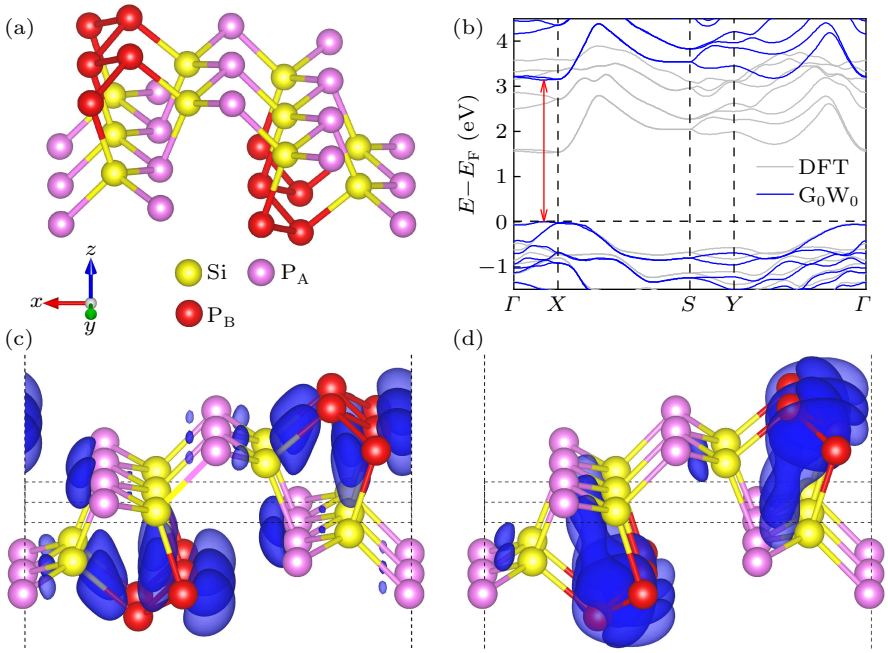


Fig. 1. (a) Crystal structure of monolayer SiP_2. (b) Electronic band structures of monolayer SiP_2 calculated using DFT with the PBE functional (grey lines) and the G_0W_0 approach (blue lines). The band gap from DFT is 1.52 eV, while G_0W_0 yields 3.14 eV (red double arrow). Real-space charge density distributions of (c) the valence band maximum (VBM) and (d) conduction band minimum (CBM). The isosurface value is set to 0.0025 $e\cdot(\text{Bohr})^{-3}$.

To explore the optical properties of monolayer SiP_2, we calculate the absorption spectra using both the GW-BSE method and the independent particle approximation (IPA) with incident light polarized along the x and y directions, as shown in Figs. 2(a) and 2(b). Compared with the IPA spectra, the GW-BSE results incorporate electron–hole Coulomb interactions, revealing multiple exciton peaks. Notably, the lowest bright exciton exhibits a binding energy of 820 meV under x-polarized light and 450 meV under y-polarized light, reflecting significant in-plane anisotropy. Additionally, a strong absorption peak appears around 3.0 eV in Fig. 2(a), with an oscillator strength even greater than those associated with lower-energy excitons. This indicates that the excitonic states in monolayer SiP_2 cannot be fully described by a simple hydrogenic model.[16] Furthermore, the most strongly bound state obtained from the BSE is a dark exciton with a binding energy of 840 meV, which is optically inactive in both polarizations, highlighting the complexity of the excitonic landscape in monolayer SiP_2.

To gain a deeper understanding of the anisotropic optical selection rules in monolayer SiP_2, we present the excitonic distribution weight $\sum_{vc}|A^{\lambda}_{vc\boldsymbol{k}}|^2$ in reciprocal space for four representative excitonic states, as illustrated in Figs. 2(d)–2(g). Here, $A^{\lambda}_{vc\boldsymbol{k}}$ is the expansion coefficient of the excitonic wavefunction $\Psi^{\lambda}(\boldsymbol{r}_e,\boldsymbol{r}_h)$, expressed as

$$\Psi^{\lambda}(\boldsymbol{r}_e,\boldsymbol{r}_h)=\sum_{vc\boldsymbol{k}}A^{\lambda}_{vc\boldsymbol{k}}\psi_{c\boldsymbol{k}}(\boldsymbol{r}_e)\psi^{*}_{v\boldsymbol{k}}(\boldsymbol{r}_h), \tag{1}$$

where $\psi_{c\boldsymbol{k}}(\boldsymbol{r}_e)$ and $\psi^{*}_{v\boldsymbol{k}}(\boldsymbol{r}_h)$ represent the quasiparticle states of electrons and holes; $\boldsymbol{r}_e$ and $\boldsymbol{r}_h$ denote the positions of electrons and holes; v and c are the indices of the valence and conduction bands; and $\boldsymbol{k}$ is the crystal momentum in the BZ. Due to in-plane anisotropic screening, the rotational symmetry of bound 2D electron–hole pairs is broken, leading to the loss of angular momentum conservation for both electrons and holes. Consequently, spherical harmonic functions are no longer eigenstates of the system, and excitonic wavefunctions cannot be classified as s, p, or d states, unlike Rydberg excitons in isotropic 2D semiconductors such as MoS_2.[16,17]

As shown in Figs. 2(d)–2(f), excitons 1 to 3 are bright under x-polarized light and are predominantly localized along the Γ–X path, where the band edges are relatively flat. This flatness facilitates the mixing of single-particle transitions, resulting in broader excitonic features in momentum space, distinct from their bulk counterparts.[24] Furthermore, exciton 4, shown in Fig. 2(g), is bright under y-polarized light and is mainly contributed by states along the X–S path near the X point, in contrast to excitons 1 to 3.

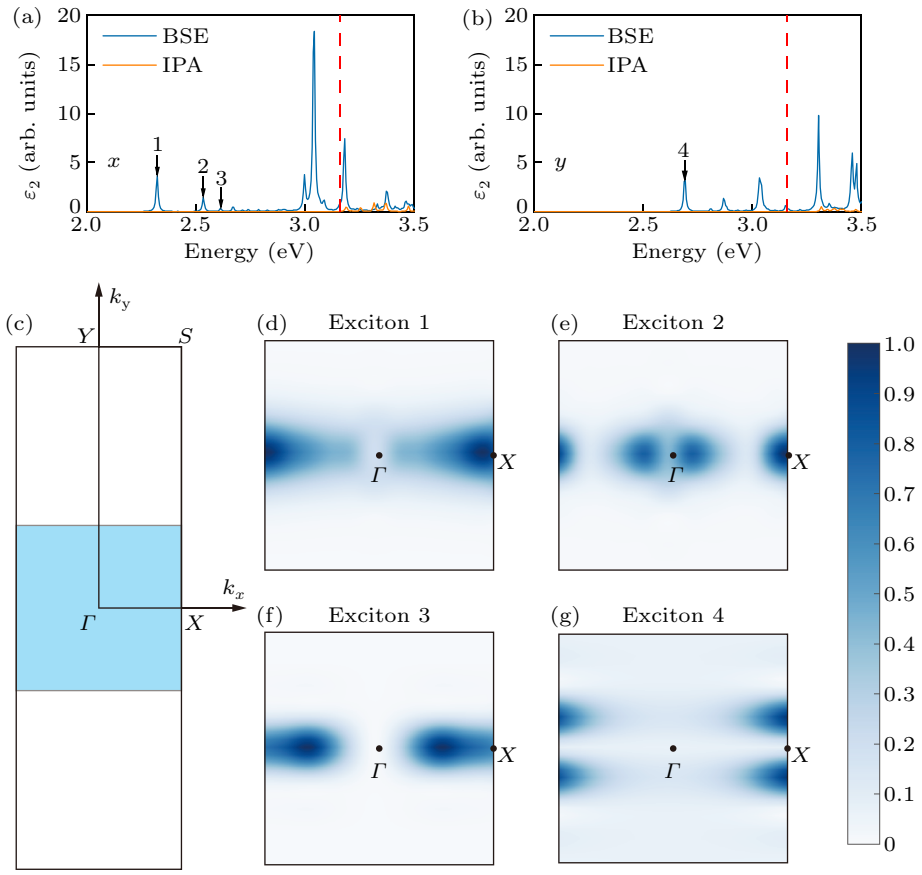


Fig. 2. (a) The imaginary part of the dielectric function for monolayer SiP_2 calculated using the BSE (blue lines) and IPA (orange lines) for the incident light polarized along the x direction. The red dashed line denotes the direct gap (3.14 eV), and the excitonic peaks from 1 to 3 at 2.32 eV, 2.53 eV, 2.61 eV are labeled. (b) Similar results as (a), but for the incident light polarized along the y direction. An additional excitonic peak 4 at 2.69 eV is labeled. (c) The first BZ of monolayer SiP_2, with the excitonic distribution weight mainly located in the blue region. (d)–(g) Excitonic distribution weights within the blue region for the four excitonic states mentioned above.

Since ε_2 is determined by $\sum_\lambda \sum_{vc\boldsymbol{k}} |A^\lambda_{vc\boldsymbol{k}} \langle v_{\boldsymbol{k}}|x(y)|c_{\boldsymbol{k}}\rangle|^2$, the anisotropic optical activity can be further understood through group theory analysis of the dipole transition matrix elements $\langle v_{\boldsymbol{k}}|x|c_{\boldsymbol{k}}\rangle$ and $\langle v_{\boldsymbol{k}}|y|c_{\boldsymbol{k}}\rangle$, where $|v_{\boldsymbol{k}}\rangle$ ($|c_{\boldsymbol{k}}\rangle$) represents the VB (CB) wavefunction at a given $\boldsymbol{k}$ point. Monolayer SiP_2 belongs to the space group $Pmc2_1$ (No. 26), which includes two fundamental symmetry operations: the mirror reflection perpendicular to the y axis (M_y) and the nonsymmorphic screw rotation along the x axis ($S_{2x} = \{C_{2x}|(\frac{1}{2},0,0)\}$). Time-reversal symmetry is also preserved in the absence of magnetism. As the Γ–X path plays a crucial role in the distribution of excitonic wavefunctions, we analyze the symmetry constraints on the dipole transition matrix elements along this path. For the matrix element $\langle v_{\boldsymbol{k}}|x|c_{\boldsymbol{k}}\rangle$ at a given $\boldsymbol{k}$ point (the case for $\langle v_{\boldsymbol{k}}|y|c_{\boldsymbol{k}}\rangle$ is similar):

$$\begin{aligned}\langle v_{\boldsymbol{k}}|x|c_{\boldsymbol{k}}\rangle &= \langle v_{\boldsymbol{k}}|(S_{2x})^{-1} S_{2x} x (S_{2x})^{-1} S_{2x}|c_{\boldsymbol{k}}\rangle \\ &= (\mu^x_{v\boldsymbol{k}})^* \mu^x_{c\boldsymbol{k}} \langle v_{\boldsymbol{k}}|x|c_{\boldsymbol{k}}\rangle, \qquad (2)\\ \langle v_{\boldsymbol{k}}|x|c_{\boldsymbol{k}}\rangle &= \langle v_{\boldsymbol{k}}|(M_y)^{-1} M_y x (M_y)^{-1} M_y|c_{\boldsymbol{k}}\rangle \\ &= (\mu^y_{v\boldsymbol{k}})^* \mu^y_{c\boldsymbol{k}} \langle v_{\boldsymbol{k}}|x|c_{\boldsymbol{k}}\rangle, \qquad (3)\end{aligned}$$

where $\mu^x_{v\boldsymbol{k}}$, $\mu^x_{c\boldsymbol{k}}$, $\mu^y_{v\boldsymbol{k}}$, and $\mu^y_{c\boldsymbol{k}}$ are the eigenvalues for the VB and CB at a specific $\boldsymbol{k}$ point under the S_{2x} and M_y symmetry operations. The matrix element $\langle v_{\boldsymbol{k}}|x|c_{\boldsymbol{k}}\rangle$ is nonzero only if both $(\mu^x_{v\boldsymbol{k}})^* \mu^x_{c\boldsymbol{k}}$ and $(\mu^y_{v\boldsymbol{k}})^* \mu^y_{c\boldsymbol{k}}$ equal 1. First-principles calculations of these eigenvalues reveal that the matrix elements vanish along the Γ–X path in both x and y directions, except at the X point. At the X point, where the bands are doubly degenerate, $\langle v_{\boldsymbol{k}}|x|c_{\boldsymbol{k}}\rangle$ is nonzero, explaining why excitons 1 to 3 are optically active under x-polarized light but inactive along the y direction. Similarly, exciton 4 exhibits nonzero dipole transition matrix elements for y-polarized light at the S point, but vanishing elements for x-polarization, consistent with its localization along the X–S path.

Having established the symmetry origin of the anisotropic optical selection rules, we analyze the $\boldsymbol{k}$-resolved excitonic distribution weights over the band structures as shown in Fig. 3 to elucidate the binding energy disparity. Exciton formation typically occurs near the electronic band edge, where both electrons and holes have low group velocities. As shown in Figs. 3(a)–3(c), excitons under x-polarized light are contributed by multiple $\boldsymbol{k}$ points along the Γ–X direction due to the flatness of the CB and VB in this region. This distribution resembles flat-band semiconductors such as V_2O_5,[20,21] where the enhanced effective mass arising from flat disper-

sion leads to significantly stronger excitonic binding. In contrast, the distribution of exciton 4 in Fig. 3(d) is predominantly localized near a $\boldsymbol{k}$ point close to X, due to strongly dispersive bands along the X–S direction. Consequently, excitons under x-polarized light exhibit higher binding energies compared to y-polarized excitons. This anisotropy is also reflected in the polarization-dependent bright excitonic transitions: the lowest-energy x-polarized transition occurs at 2.32 eV, while the y-polarized counterpart appears at 2.69 eV. These distinct optical responses highlight the potential of monolayer SiP_2 for directionally tunable optoelectronic and electroluminescent devices.

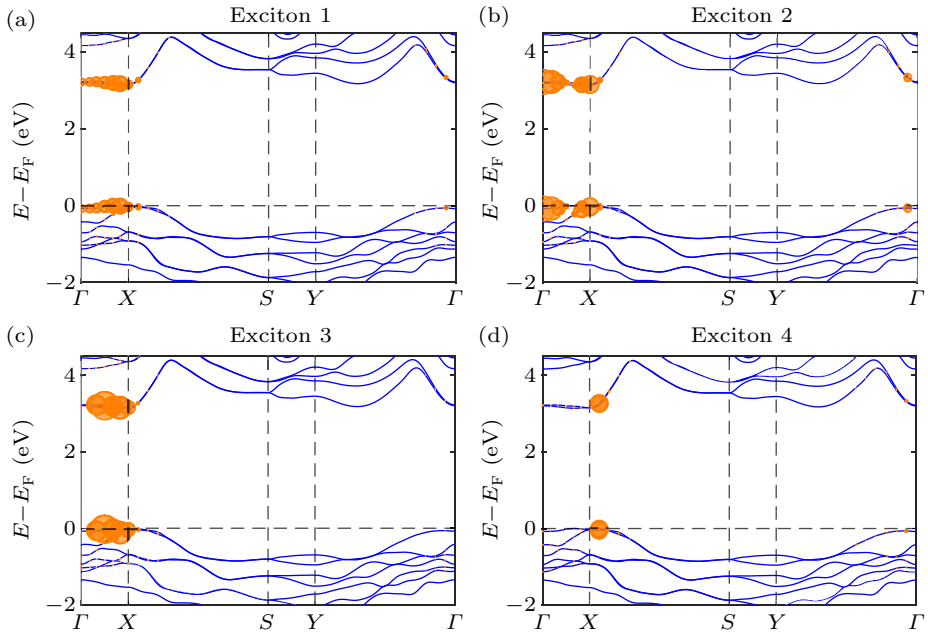


Fig. 3. (a)–(d) Electronic band structures of monolayer SiP_2 with excitonic distribution weights projected for the four representative excitonic states. The size of the orange circles indicates the magnitude of the excitonic distribution weight at each $\boldsymbol{k}$ point.

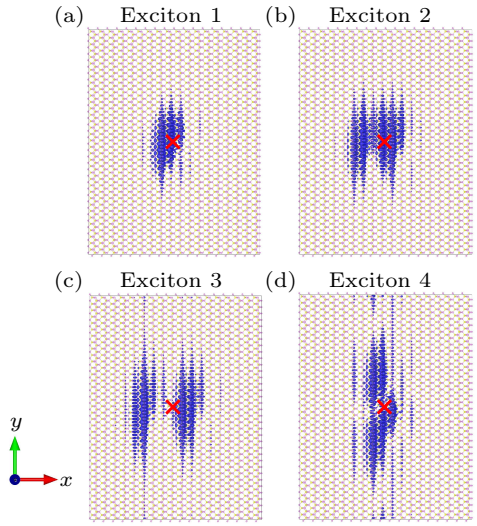


Fig. 4. (a)–(d) Modulus squared of the excitonic wavefunctions for the four bright excitons in real space, calculated using GW-BSE. Red crosses indicate the positions of the holes.

To determine the exciton size and character (Wannier–Mott or Frenkel) in monolayer SiP_2, we examine the squared modulus of the excitonic wavefunction $|\Psi^{\lambda}(\boldsymbol{r}_e, \boldsymbol{r}_h^0)|^2$, representing the real-space distribution of the electron with the hole fixed at $\boldsymbol{r}_h^0$. These GW-BSE results are presented in Fig. 4, where red crosses denote the positions of the holes. The spatial distributions indicate that all four excitons in monolayer SiP_2 are of the Wannier–Mott type and highly anisotropic. Moreover, the exciton radius (effective Bohr radius) increases as the exciton binding energy decreases, reflecting the weakening of the electron–hole Coulomb interaction for excitons with lower binding energies.

4. Conclusion

Using first-principles GW-BSE calculations, we systematically investigate the electronic band structures and excitonic properties of monolayer SiP_2 with an orthorhombic 2D crystal structure. The G_0W_0 approximation reveals a direct band gap of 3.14 eV, with excitons exhibiting a unique hybrid-dimensional character, similar to bulk SiP_2 but with enhanced many-body effects and stronger electron–hole interactions. This is manifested in the optical spectra through strongly anisotropic excitonic features: the first bright exciton shows a binding energy of 840 meV under x-polarized light but 450 meV under y-polarized light, governed by the polarization-dependent optical selection rules imposed by crystal symmetry. The anisotropy arises from two distinct regimes: flat-band excitons under x-polarized light with extended $\boldsymbol{k}$-space distribution and enhanced electron–hole interactions, and conventional excitons under y-polarized light localized at a single $\boldsymbol{k}$ point. These two excitonic regimes collec-

tively modulate the electron–hole interaction strength through direction-dependent effective masses. Our findings highlight the potential of monolayer SiP_2 as a promising platform for polarization-sensitive and directionally tunable optoelectronic applications.

Acknowledgments

This work is supported by the National Natural Science Foundation of China (Grant Nos. 12234011 and 12374053) and the National Key Research and Development Program of China (Grant No. 2024YFA1409100).

References

[1] Wilson N P, Yao W, Shan J and Xu X 2022 *Nature* **599** 383
[2] Fu Q, Hu Z, Zhou M, Lu J and Ni Z 2021 *Laser Photonics Rev.* **15** 2000587
[3] Wang S, Wang J, Zhao W, Giustiniano F, Chu L, Verzhbitskiy I, Yong J Z and Eda G 2017 *Nano Lett.* **17** 5156
[4] Bai Y, Wang Y and Meng S 2024 *Phys. Rev. Lett.* **133** 046903
[5] Dai Z, Lian C, Lafuente-Bartolome J and Giustino F 2024 *Phys. Rev. Lett.* **132** 036902
[6] Yao J, Sheng H, Zhang R, Pang R, Zhou J J, Wu Q, Weng H, Dai X, Fang Z and Wang Z 2024 *Chin. Phys. Lett.* **41** 097101
[7] Onida G, Reining L and Rubio A 2002 *Rev. Mod. Phys.* **74** 601
[8] Cudazzo P, Tokatly I V and Rubio A 2011 *Phys. Rev. B* **84** 085406
[9] Lian C, Zhang S J, Hu S Q, Guan M X and Meng S 2020 *Nat. Commun.* **11** 43
[10] Yuan L and Huang L 2015 *Nanoscale* **7** 7402
[11] Mueller T and Malic E 2018 *npj 2D Mater. Appl.* **2** 29
[12] Chan Y, Haber J B, Naik M H, Neaton J B, Qiu D Y, da Jornada F H and Louie S G 2023 *Nano Lett.* **23** 3971
[13] Lin Y, Chan Y, Lee W, Lu L S, Li Z, Chang W H, Shin C K, Kaindl R A and Louie S G 2022 *Phys. Rev. B* **106** L081117
[14] Sui X, Wang H, Liang C, Zhang Q, Bo H, Wu K, Zhu Z, Gong Y, Yue S, Chen H, Shang Q, Mi Y, Gao P, Zhang Y, Meng S and Liu X 2022 *Nano Lett.* **22** 5651
[15] Liu X B, Hu S Q, Chen D, Guan M, Chen Q and Meng S 2022 *Nano Lett.* **22** 4800
[16] Qiu D Y, Da Jornada F H and Louie S G 2013 *Phys. Rev. Lett.* **111** 216805
[17] Qiu D Y, Da Jornada F H and Louie S G 2016 *Phys. Rev. B* **93** 235435
[18] Chernikov A, Berkelbach T C, Hill H M, Rigosi A, Li Y, Aslan B, Reichman D R, Hybertsen M S and Heinz T F 2014 *Phys. Rev. Lett.* **113** 076802
[19] Dong S, Chen Y, Qu H, Lou W and Chang K 2025 *Phys. Rev. Lett.* **134** 066602
[20] Garcia C, Radha S K, Acharya S and Lambrecht W R L 2024 *Phys. Rev. B* **110** 085102
[21] Gorelov V, Reining L, Feneberg M, Goldhahn R, Schleife A, Lambrecht W R L and Gatti M 2022 *npj Comput. Mater.* **8** 94
[22] Dai X, Qin F, Qiu C, Zhou L, Huang J, Cheng F, Bi X, Zhang C, Li Z, Tang M, Wu S, Zhao X, Lu Y, Gou H and Yuan H 2023 *Nano Res.* **16** 1107
[23] Li Z, Huang J, Zhou L, Xu Z, Qin F, Chen P, Sun X, Liu G, Sui C, Qiu C, Lu Y, Gou H, Xi X, Ideue T, Tang P, Iwasa Y and Yuan H 2023 *Nat. Commun.* **14** 5568
[24] Cheng F, Huang J, Qin F, Zhou L, Dai X, Bi X, Zhang C, Li Z, Tang M, Qiu C, Lu Y, Gou H and Yuan H 2022 *Nano Res.* **15** 7378
[25] Zhou L, Huang J, Windgaetter L, Ong C S, Zhao X, Zhang C, Tang M, Li Z, Qiu C, Latini S, Lu F, Wu D, Gou H, Wee A T S, Hosono H, Louie S G, Tang P, Rubio A and Yuan H 2022 *Nat. Mater.* **21** 773
[26] Matta S K, Zhang C, Jiao Y, O'Mullane A and Du A 2018 *Nanoscale* **10** 6369
[27] Zhou J, Cai T Y and Ju S 2020 *Phys. Rev. Res.* **2** 033288
[28] Zhou R, Sui L, Liu X, Liu K, Guo D, Zhao W, Song S, Lv C, Chen S, Jiang T, Cheng Z, Meng S and Shan C 2023 *Nat. Commun.* **14** 1310
[29] Caruso F, Filip M R and Giustino F 2015 *Phys. Rev. B* **92** 125134
[30] Huang T A, Zacharias M, Lewis D K, Giustino F and Sharifzadeh S 2021 *J. Phys. Chem. Lett.* **12** 3802
[31] Xia F, Wang H, Xiao D, Dubey M and Ramasubramaniam A 2014 *Nat. Photonics* **8** 899
[32] Yang L, Deslippe J, Park C H, Cohen M L and Louie S G 2009 *Phys. Rev. Lett.* **103** 186802
[33] Gomes L C, Trevisanutto P E, Carvalho A, Rodin A S and Castro Neto A H 2016 *Phys. Rev. B* **94** 155428
[34] Ying X and Law K T 2024 arXiv:2407.00325 [cond-mat.mes-hall]
[35] Rozzi C A, Varsano D, Marini A, Gross E K U and Rubio A 2006 *Phys. Rev. B* **73** 205119
[36] Giannozzi P, Baroni S, Bonini N, *et al*. 2009 *J. Phys.: Condens. Matter* **21** 395502
[37] Perdew J P, Burke K and Ernzerhof M 1996 *Phys. Rev. Lett.* **77** 3865
[38] Schlipf M and Gygi F 2015 *Comput. Phys. Commun.* **196** 36
[39] Iraola M, Mañes J L, Bradlyn B, Horton M K, Neupert T, Vergniory M G and Tsirkin S S 2022 *Comput. Phys. Commun.* **272** 108226
[40] Sangalli D, Ferretti A, Miranda H, *et al*. 2019 *J. Phys.: Condens. Matter* **31** 325902
[41] Marini A, Hogan C, Grüning M and Varsano D 2009 *Comp. Phys. Comm.* **104** 180
[42] Wolf D, Keblinski P, Phillpot S R and Eggebrecht J 1999 *J. Chem. Phys.* **110** 8254
[43] Rohlfing M and Louie S G 2000 *Phys. Rev. B* **62** 4927
[44] Chen Y, Lou W K, Yang W and Chang K 2025 *New J. Phys.* **27** 023026